APPLIED GEOPHYSICS, Vol.13, No.1 (March 2016), P. 59-68, 4 Figures.
DOI:10.1007/s11770-016-0533-5

Regional magnetic anomaly fields: 3D Taylor polynomial and surface spline models*

Feng Yan♦[1,2], Jiang Yong[1], Jiang Yi[1], Li Zheng[1], Jiang Jin[1], Liu Zhong-Wei[1], Ye Mei-Chen[1], Wang Hong-Sheng[1], and Li Xiu-Ming[1]

Abstract: We used data from 1960.0, 1970.0, 1980.0, 1990.0, and 2000.0 to study the geomagnetic anomaly field over the Chinese mainland by using the three-dimensional Taylor polynomial (3DTP) and the surface spline (SS) models. To obtain the pure anomaly field, the main field and the induced field of the ionospheric and magnetospheric fields were removed from measured data. We also compared the SS model anomalies and the data obtained with Kriging interpolation (KI). The geomagnetic anomaly distribution over the mainland was analyzed based on the SS and 3DTP models by transferring all points from 1960.0−1990.0 to 2000.0. The results suggest that the total intensity F anomalies estimated based on the SS and KI for each year are basically consistent in distribution and intensity. The anomalous distributions in the X-, Y-, and Z-direction and F are mainly negative. The 3DTP model anomalies suggest that the intensity in the X-direction increases from −100 nT to 0 nT with longitude, whereas the intensity in the Y-direction decreases from 400 nT to 20 nT with longitude and over the eastern mainland is almost negative. The intensity in the Z-direction and F are very similar and in most areas it is about −50nT and higher in western Tibet. The SS model anomalies overall reflect the actual distribution of the magnetic field anomalies; however, because of the uneven distribution of measurements, it yields several big anomalies. Owing to the added altitude term, the 3DTP model offers higher precision and is consistent with KI.
Keywords: Magnetic anomaly field, three-dimensional Taylor polynomial, surface spline, CM4

Introduction

The amplitude of the magnetic anomaly field, denoted as lithospheric magnetic field or crustal field, reaches several thousands of nT during a magnetic storm or solar flare, and may appear static or locally variable. The study of global or regional anomaly fields yields information regarding tectonics, geological structures, navigation, and mineral exploration.

Typically, magnetic anomaly fields are studied by using data from geophysical observatories, research

Manuscript received by the Editor December 12, 2014; revised manuscript received February 18, 2016.
* This work was supported by the National Natural Science Foundation of China (No. 41404053), Special Project for Meteo-Scientific Research in the Public Interest (No. GYHY201306073), Natural Science Foundation of Jiangsu Province (No. BK20140994), Natural Science Foundation of Higher Education Institutions of Jiangsu Province (No. 14KJB170012) and Training Program of Innovation and Entrepreneurship for Undergraduates of NUIST (No. 201510300178).
1. The College of Mathematics and Statistics, Nanjing University of Information Science & Technology, Nanjing 210044, China.
2. Sate Key Laboratory of Space Weather, Chinese Academy of Sciences, Beijing 100080, China.
♦Corresponding Author: Feng Yan (Email: frank_feng8848@163.com)

vessels and planes, and satellites. Many sophisticated global models have been generated since the Magsat satellite was launched in 1979, e.g., comprehensive models (CMs) (Langel et al., 1996; Sabaka et al., 2002; Sabaka et al., 2004), lithospheric magnetic field model (MFDs) (Maus et al., 2007; Maus et al., 2008), and the NGDC-720 lithospheric magnetic model (NGDC720) (Maus, 2010). These models offer high truncation level, high resolution, and reasonable separation of the geomagnetic sources. They are being extensively used; however, these satellite-based models have two fundamental shortcomings. First, the ground-based observatories that contribute to the models are not unevenly distributed. Second, most satellite data are obtained between 300 km and 800 km altitude and, at this level, the anomaly field attenuates rapidly and consequently affects the model precision.

Many have studied the magnetic anomalies over the Chinese mainland by ordinary regional models, such as Taylor polynomial (TP) (An, 1992a, 1992b, 2000; Xu et al., 2003), surface spline (SS) (Gao et al., 2006; Feng et al., 2010a), spherical cap harmonics (SCH) (An, 2003; Gu et al., 2004, 2006a, 2006b), rectangular harmonics (RH) (Wang et al., 1999), the NOC model (Gu et al., 2009), etc. Tschu and Xu (1985) studied local geomagnetic structures by RH and derived the embedded anomaly model of Northern China for 1970. Gao et al (2005) combined survey data, TPs, SCH, and IGRF to derive the anomaly model for China in 2003. However, after comparing the anomaly distributions between global and regional models, several differences are obvious. To date, studies that combine continuously measured points and regional and global models over mainland China are rare.

The anomaly field is generally thought to be static. However, owing to instrument improvements and modeling advances, the problems of uneven data distribution and noise are being overcome. To obtain reliable anomaly field data, high-density observations are necessary. Considering the above, fourth-generation comprehensive models (CM4) should be used to obtain the anomaly values, and TPs are widely used to fit regional data because of their computational simplicity and suitability to describe the magnetic field at medium to small scales (Feng et al., 2010b); nevertheless, they lack altitude information. It is known that the geomagnetic field intensity rapidly decreases with altitude, especially field anomalies. The measured decay rate of the total intensity F is about 20nT/km. Liu et al. (2011) constructed the three-dimensional Taylor polynomial (3DTP) model to take into account the altitude. In this study, we adopted the 3DTP model to study the distribution of magnetic anomalies over mainland China and also used the SS method because of its interpolation and expression capabilities of complex regional geomagnetic data (Feng et al., 2010b). We created regional models by using SS for 1960.0, 1970.0, 1980.0, 1990.0, and 2000.0 and then analyzed and compared the magnetic anomalies by using Kriging interpolation (KI). To investigate the distribution during 1960.0–2000.0, we assumed that the anomaly values during this period did not change and all anomalies were transferred to 2000.0. Subsequently, the anomalies in the X-direction (North), Y-direction (East), and Z-direction (vertical) were analyzed. The anomaly distributions based on two regional models are compared to the distribution obtained with KI. The results of this study are of theoretical and practical significance to geophysical research over mainland China.

Data and methods

Data

Ground-based data are mainly used in this study; 445 observations for declination D, inclination I, and the horizontal element H in 1960.0; 1887 observations for D, I, and H in 1970.0; 255 D, I, and F in 1980.0; 137 observations for D, I, and F in 1990.0; and 156 observations for D, I, and F in 2000.0. The data were provided by the Institute of Geology and Geophysics, Chinese Academy of Sciences.

Diurnal variations and disturbances at the stations were eliminated by referring to the nearest magnetic observatories, and the station values were updated to a common point in time (e.g., 1960.0) by using the hourly values at the reference observatories. To reflect the actual anomalous distributions, many points in each period were adopted.

We assumed that anomaly values did not vary with time and all available values from 1960.0, 1970.0, 1980.0, and 1990.0 were concentrated into 2000.0 to study the overall distribution during 1960.0–2000.0. Thus, there were 277 overlap points and we retained the ones that were closer to the corresponding lithospheric field of CM4. Finally, 2730 points were obtained and are shown in Figure 1.

In this study, we indirectly used satellite data and adopted the geomagnetic scalar data (F) provided by the POGO and CHAMP satellites, and the scalar and vector data (X, Y, Z) provided by Magsat and Oersted

during 1960−2000. The total number of points was greater than 1600000 and to improve the precision of the calculations, the vector data of Magsat were reselected. During the magnetic quiet conditions in which $K_p \leq 1^0$ for the time of the observation and $K_p \leq 2^0$ for the previous 3 h interval, the vector data were selected for 20 arcsec accuracy. The Oersted and CHAMP data were selected for quiet conditions ($K_p \leq 1^+$) for the time of the observation and $K_p \leq 2^0$ for the previous 3 h interval. In addition, $|D_{st}| \leq 20$ nT.

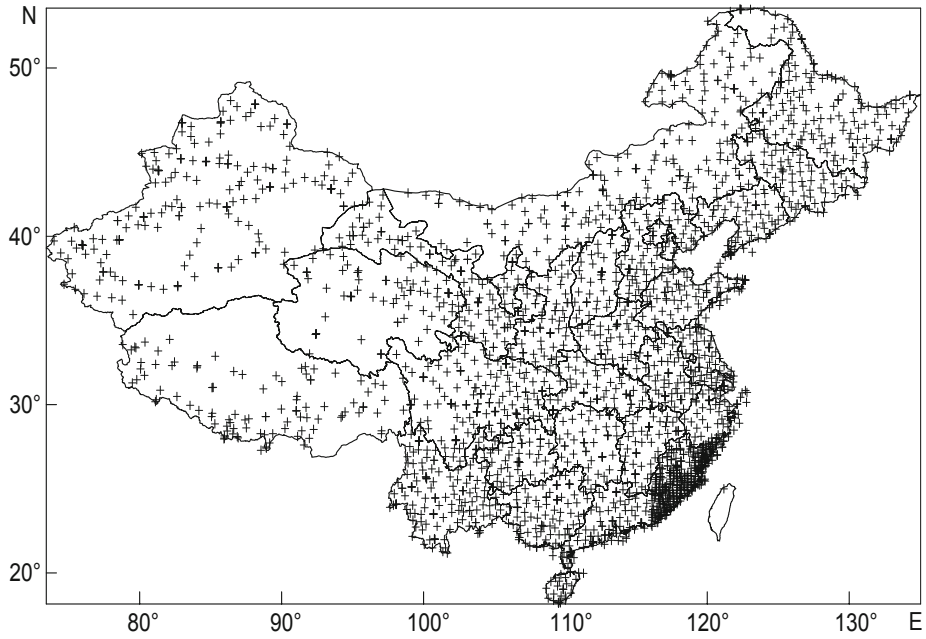

Fig.1 Distribution of the measurement points over the Chinese mainland during 1960.0−2000.0.

Methods

Although the external ionospheric and magnetospheric magnetic fields were filtered, the data contained at least two sources of noise: the main field and induced fields generated from currents in the ionosphere and magnetosphere. To obtain the pure anomaly field, these two sources of noise were removed with the following equation

$$B_a = B_m - B_c - B_i, \tag{1}$$

where B_a is the anomaly field, B_m are the measured data, B_c is the core field, and B_i is the induced field from the external field. B_c and B_i are modeled by CM4 and, then, the anomaly models can be derived by the SS and 3DTP.

1. The CM4 model

CM4 is an excellent model in terms of the separation of the different geomagnetic sources. Based on ground-based and satellite data and iteratively reweighted least squares (IRLS) with Huber weights, the geomagnetic field can be separated from the main field, lithospheric field, and the ionospheric and magnetospheric fields as well as the induced fields.

The main field is removed from the measurements to obtain the anomaly field. The systems responsible for the main field and lithospheric magnetic fields lie entirely below regions sampled by permanent observatories and satellites. Therefore, assuming that the temporal variations of terms with $n > 15$ is negligible, the final working expression for the potential of these fields is (Langel et al., 1982)

$$V_{cl}(t,L) = \Re[a\sum_{n=1}^{13}\sum_{m=0}^{n}\sum_{q=0}^{13}(\frac{a}{r})^{n+1}\gamma_{nq}^{m}Y_{nq}^{m}(t,\theta,\phi) + a\sum_{n=16}^{65}\sum_{m=0}^{n}(\frac{a}{r})^{n+1}\gamma_{n}^{m}Y_{n}^{m}(\theta,\phi)], \tag{2}$$

$$Y_{nq}^{m}(t,\theta,\phi) = \begin{cases} Y_n^m(\theta,\phi), q=0 \\ Y_n^m(\theta,\phi)\int_{t_0}^{t} b_q(\tau)d\tau, q>0 \end{cases},$$

and

$$Y_n^m(\theta,\phi) = P_n^m(\cos\theta)\exp(im\phi),$$

where a is the mean radius of the Earth (6371.2 km), r

is the distance between the measurement point and the Earth's core, L is the position vector, θ is the colatitude, ϕ is the longitude, Y_n^m and P_n^m are the Schmidt-normalized surface spherical harmonic and associated Legendre function of degree n and order m, the $\Re\{\cdot\}$ operation only uses the real part of the expression, and γ_n^m are unique complex expansion coefficients, which are also known as Gauss coefficients. They are related to the typical Gauss coefficients g_n^m and h_n^m according to $\gamma_n^m = g_n^m - ih^m$, where t is the universal time and $t_0 = 1980$. $b_q(\tau)$ is the qth cubic B-spline of the expansion. Equation 2 expands the truncation level of the spherical harmonic to 15, where the main field is dominant.

To obtain the pure anomaly field, the induced field from the ionosphere and magnetosphere are calculated and then removed by CM4.

The ionospheric current at $h = 110$ km altitude yields the equivalent induced current inside the Earth and can be approximated by the gradients of potential functions. The basis functions of the ionospheric field and its induced fields can be represented by a set of potential functions reflecting a single spatial harmonic modulated by single seasonal and diurnal periods. For regions $a \le r \le a + h$ and $r > a + h$, these functions are (Olsen, 1993)

$$\begin{aligned} &V_{\text{ion}}(t,t_{\text{mut}},L) \\ &= \Re\{\sum_{s=-2}^{2}\sum_{p=0}^{4}\sum_{l=p-1}^{p+1}\sum_{k=\max(1,|l|)}^{|l|+40}\tilde{\varepsilon}_{ksp}^{l} \\ &\times\sum_{n=1}^{60}\sum_{m=-\min(n,12)}^{\min(n,12)}[(d_{kn,\text{e}}^{lm})^{*}S_{nsp,\text{e}}^{m}(t,t_{\text{mut}},L) \\ &+(f_{knsp}^{lm})^{*}S_{nsp,\text{i}}^{m}(t,t_{\text{mut}},L)]\}, \end{aligned} \tag{3}$$

$$\begin{aligned} &V_{\text{ion}}^{'}(t,t_{\text{mut}},L) \\ &= \Re\{\sum_{s=-2}^{2}\sum_{p=0}^{4}\sum_{l=p-1}^{p+1}\sum_{k=\max(1,|l|)}^{|l|+40}\tilde{\varepsilon}_{ksp}^{l} \\ &\times\sum_{n=1}^{60}\sum_{m=-\min(n,12)}^{\min(n,12)}[(f_{knsp}^{lm})^{*}+(z_{kn}^{lm})^{*}]\times S_{nsp,\text{i}}^{m}(t,t_{\text{mut}},L)\}, \end{aligned} \tag{4}$$

where t_{mut} is the magnetic universal time, $f_{knsp}^{lm} = q_{nnsp}^{mm} d_{kn,e}^{lm}$,

$$z_{kn}^{lm} = -(\frac{n}{n+1})(\frac{a+h}{a})^{n+2} d_{kn}^{lm},\ d_{kn,e}^{lm} = (\frac{a}{a+h})^{n-1} d_{kn}^{lm},$$

and d_{kn}^{lm} is obtained by standard spherical transform. The coefficients $\tilde{\varepsilon}_{ksp}^{l}$ of the quasi-dipole field are $\tilde{\varepsilon}_{ksp}^{l} = \tilde{\varepsilon}_{ksp}^{l}(1 + NF_{10.7})$, $(f_{knsp}^{lm})^{*} = f_{knsp}^{-lm}$, and $F_{10.7}$ is the solar radiation flux index; furthermore, $N = 14.85 * 10^{-3}(10^{-22} W \cdot m^{-2} Hz^{-1})^{-1}$.

The magnetospheric field and its associated induced fields are expressed as (Sabaka et al., 2002)

$$\begin{aligned} &V_{\text{mag}}(t,t_{\text{mut}},L) \\ &= \Re\{\sum_{s=-2}^{2}\sum_{p=0}^{5}\sum_{l=p-1}^{p+1}\sum_{k=\max(1,|l|)}^{|l|+K(p-l)}\mu_{ksp}^{l}\begin{bmatrix}S_{ksp,\text{e}}^{l}(t,t_{\text{mut}},L) \\ +(q_{kksp}^{ll})^{*}S_{ksp,\text{i}}^{l}(t,t_{\text{mut}},L)\end{bmatrix} \\ &+\sum_{s=-2}^{2}\sum_{p=0}^{5}\sum_{l=p-1}^{p+1}\sum_{k=\max(1,|l|)}^{1}\mu_{ksp,D_{st}}^{l}\times D_{st}[S_{ksp,\text{e}}^{l}(t,t_{\text{mut}},L) \\ &+(q_{kksp,D_{st}}^{ll})^{*}S_{ksp,\text{i}}^{l}(t,t_{\text{mut}},L)]\}, \end{aligned} \tag{5}$$

where D_{st} is the ring-current index, l is selected within a narrow band about p, the maximum k is at a constant offset, and K is a function of the local versus nonlocal time. There is also the transform matrix Q in the parameterization process, and s, p and D_{st} are indexed by Q.

2. Three-Dimensional Taylor Polynomial model

The TP model is two dimensional. Because the geomagnetic intensity decreases with increasing altitude, there is precision loss from −10 nT to 180 nT with increasing altitude from −0.15 km to 8.8 km over the Chinese mainland (http://www.ngdc.noaa.gov/mgg/topo/).

We adopt the 3DTP model (Liu et al., 2011) to model the anomaly field. Compared to the typical TP model, an altitude term is added and the 3DTP is fully expanded.

The expression for the 3DTP is (Liu et al., 2011)

$$W = \sum_{n=0}^{\text{N}}\sum_{m=0}^{\text{N}}\sum_{k=0}^{\text{N}} A_{nmk}(\varphi-\varphi_0)^n(\lambda-\lambda_0)^m(h-h_0)^k, \tag{6}$$

where W is any geomagnetic element, N is the truncation level, ϕ, λ, and h are the latitude, longitude, and altitude of each measurement point, respectively, and ϕ_0, λ_0, and h_0 represent the expansion origin $\phi_0 = 36.0^\circ$, $\lambda_0 = 104.5^\circ$, $h_0 = 2.21$ km. A_{nmk} are coefficients to be derived by standard least squares methods, and there are N^3 coefficients for each model.

The 3DTP model has at least two advantages. First, the effect of the altitude on the geomagnetic intensity is compensated and, second, it can reflect more geomagnetic information owing to its full expansion.

3. Surface spline model

The SS model is a regional model that is based on linear interpolation and is often used in complex geomagnetic situations, such as magnetic anomaly fields.

TP has several shortcomings, such as the relatively flat, simple structure (low truncation level), and numerical instability (high truncation level). In contrast, the SS is not only relatively stable but can perfectly

interpolate regional complex anomalies. Therefore, the SS and 3DTP models, to some extent, complement each other and are well suited for this study. The expressions for the SS model are (Gao et al., 2006)

$$W = a_0 + a_1 x + a_2 y + \sum_{i=1}^{M} F_i r_i^2 \ln(r_i^2 + \varepsilon), \quad (7)$$

$$\sum_{i=1}^{M} F_i = \sum_{i=1}^{M} x_i F_i = \sum_{i=1}^{M} y_i F_i = 0, \quad (8)$$

where W is any geomagnetic element, x and y are the latitude and longitude of each survey point, respectively, $r_i^2 = (x_i - x)^2 + (y_i - y)^2$, M is the number of points, a_0, a_1, a_2, and F_i are the coefficients to be derived, ε represents small values that control the changes on the surface curvature, and $\varepsilon = 1*10^{-7}$. The model has M + 3 coefficients.

Results

Because of space limitations, we only consider and analyze F and then show the distributions of the elements in the X-, Y-, and Z-direction during 1960.0–2000.0 based on the SS and 3DTP models.

Anomaly distribution of F in all epochs

The SS model that is based on the liner interpolation of all points can describe regional and complex geomagnetic distributions (Feng et al., 2010b), especially the magnetic anomalies. However, the uneven distribution of measurement points may create artifacts. To verify the SS model, we use KI to express the spatial variation and minimize the prediction error, and compare the SS and KI data. It is also known that any regional model shows more or less boundary effects owing to the lack of measured data outside the study region. After many tests, the results suggested that we obtain good control by using the method of uniform adding (UA); therefore, different numbers of complementary points are chosen for each year to minimize the boundary effects. In this study, we are primarily concerned with anomalies; thus, the corresponding lithospheric field values of CM4 are adopted as complementary points.

We show the F anomalies in Figure 2.

Theoretically, the distributions of F based on the SS model for all years should be close to the distributions that are based on KI. According to Figure 2, the F anomalies are mainly negative over mainland China. Figure 2a shows a negative anomaly of −550 nT in northeastern Inner Mongolia, and four positive anomalies in southern Inner Mongolia, northern Sichuan, southern Shanxi, and northeastern Yunnan; the maximum extreme points are 2080 nT, 1750 nT, 2690 nT, and 1010 nT. The anomaly distribution in Figure 2f shows anomalies at similar locations but the values are higher and are about −2600 nT, 2070 nT, 1440, 2690 nT, and 940 nT. For 1970.0, the two figures are consistent, with a negative anomaly of about −6000 nT by KI and −4900 nT by SS in northeastern Hebei and two positive anomalies about 2670 nT and 2450nT by KI and 2490 nT and 2240 nT SS in southern Shanxi and southeastern Zhejiang. Figure 2c shows a positive and a negative anomaly at about 2740 nT and −790 nT lies in southern Shanxi and western Tibet. The anomalies in Figure 2c are at nearly the same locations but have absolute intensities beyond 5000 nT in northeastern Inner Mongolia. The same is seen for 1990.0. Figure 2d shows a positive and a negative anomaly at about 770 nT and −580nT in northeastern Inner Mongolia and eastern Tibet, respectively. In Figure 2i, the pair of positive and negative anomalies has absolute values greater than 10000 nT in northeastern Inner Mongolia but no obvious anomaly in eastern Tibet. Both figures for year 2000.0 show consistent intensity and distribution, with a positive anomaly at about 700 nT in Beijing and a negative anomaly at about −600nT in eastern Tibet.

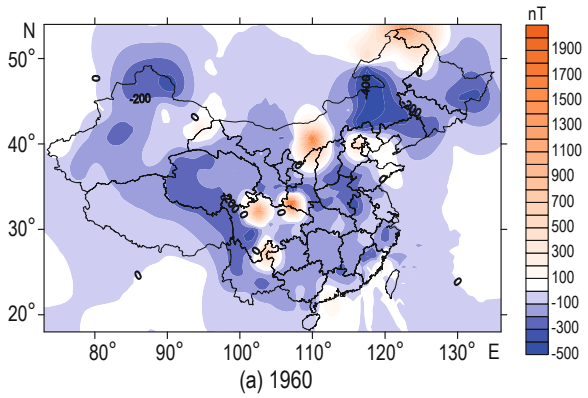

(a) 1960

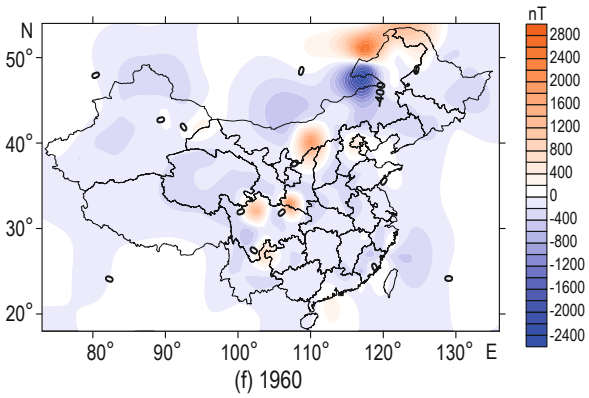

(f) 1960

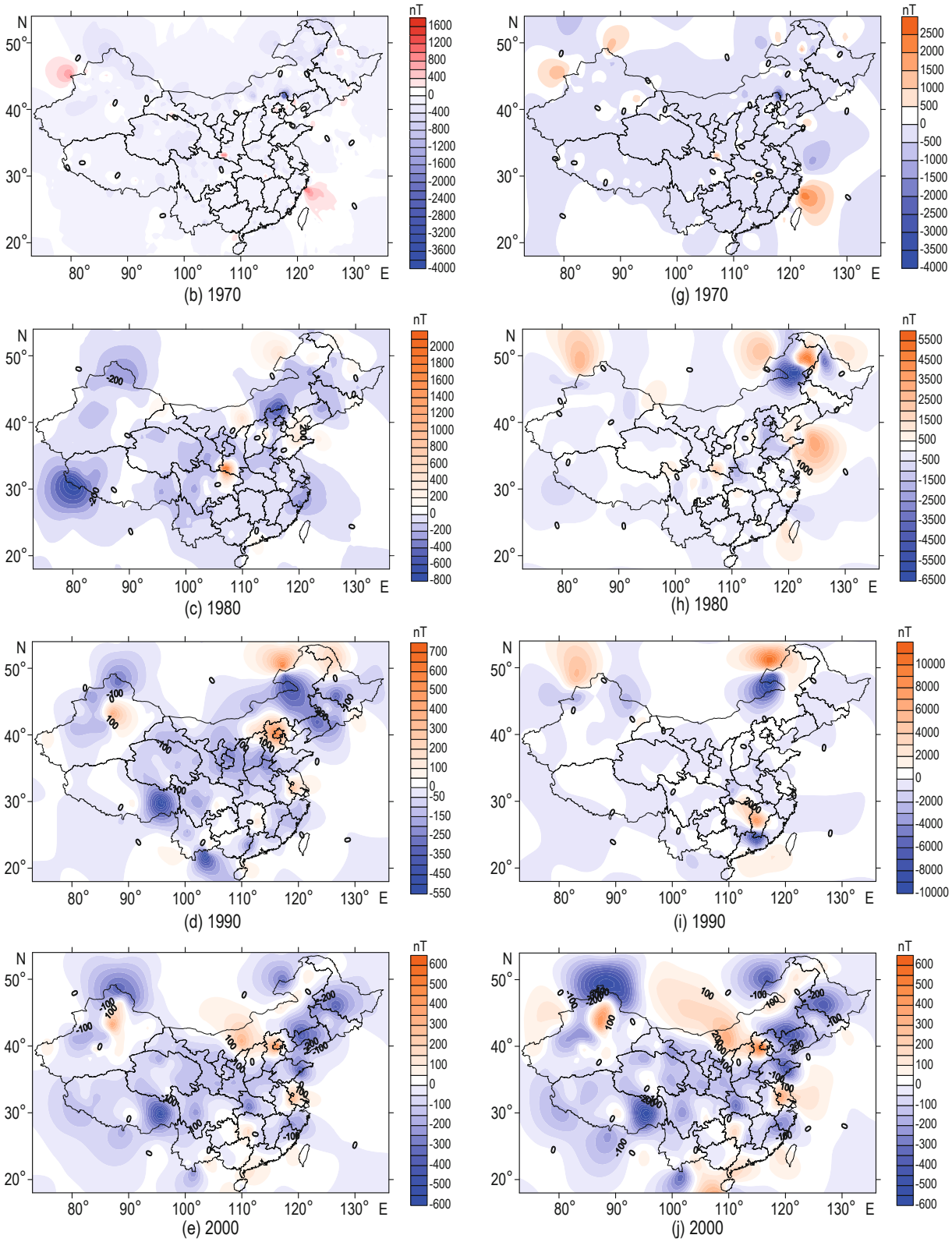

Fig.2 Anomaly distribution of F by KI (left) and SS (right). Magnetic intensity unit: nT

Both datasets in Figure 2 show consistent distributions and intensities, especially for 1960.0, 1970.0, and 2000.0. Although there are small differences in the distribution of the anomalies, e.g., the intensity of the anomalies by SS are higher than KI, they are similar in terms of the overall distribution characteristics and

locations of the anomalies. For example, a pair of positive and negative anomalies is in northeastern Inner Mongolia and a high positive anomaly is in Beijing. Considering the good distribution of measurement points in each year and the characteristics of KI, the results suggest that the SS model can reflect the magnetic anomalies over the mainland.

Overall anomaly distribution during 1960.0–2000.0

The distributions of the magnetic anomalies are close for all years. Owing to the problems mentioned in the introduction, there are, however, differences in the distributions of each year. To solve this problem, we consider all measurement points for a specific year and use numerical modeling to examine the distribution of anomalies over the mainland.

For the period 1960.0–2000.0, the available measurements are 2730. Considering the stability of the results and the boundary effects, 150 complementary points outside the country are added by the UA method after the initial comparison. First, we compare the distribution in the X-, Y-, and Z-direction and F by SS and KI. The two datasets are shown in Figure 3.

Figure 3 shows that the anomalous distributions are mainly negative. The extreme intensities based on the SS are nearly one order of magnitude higher than KI; nevertheless, by carefully comparing the two kinds of figures, we find that the overall distribution trends are

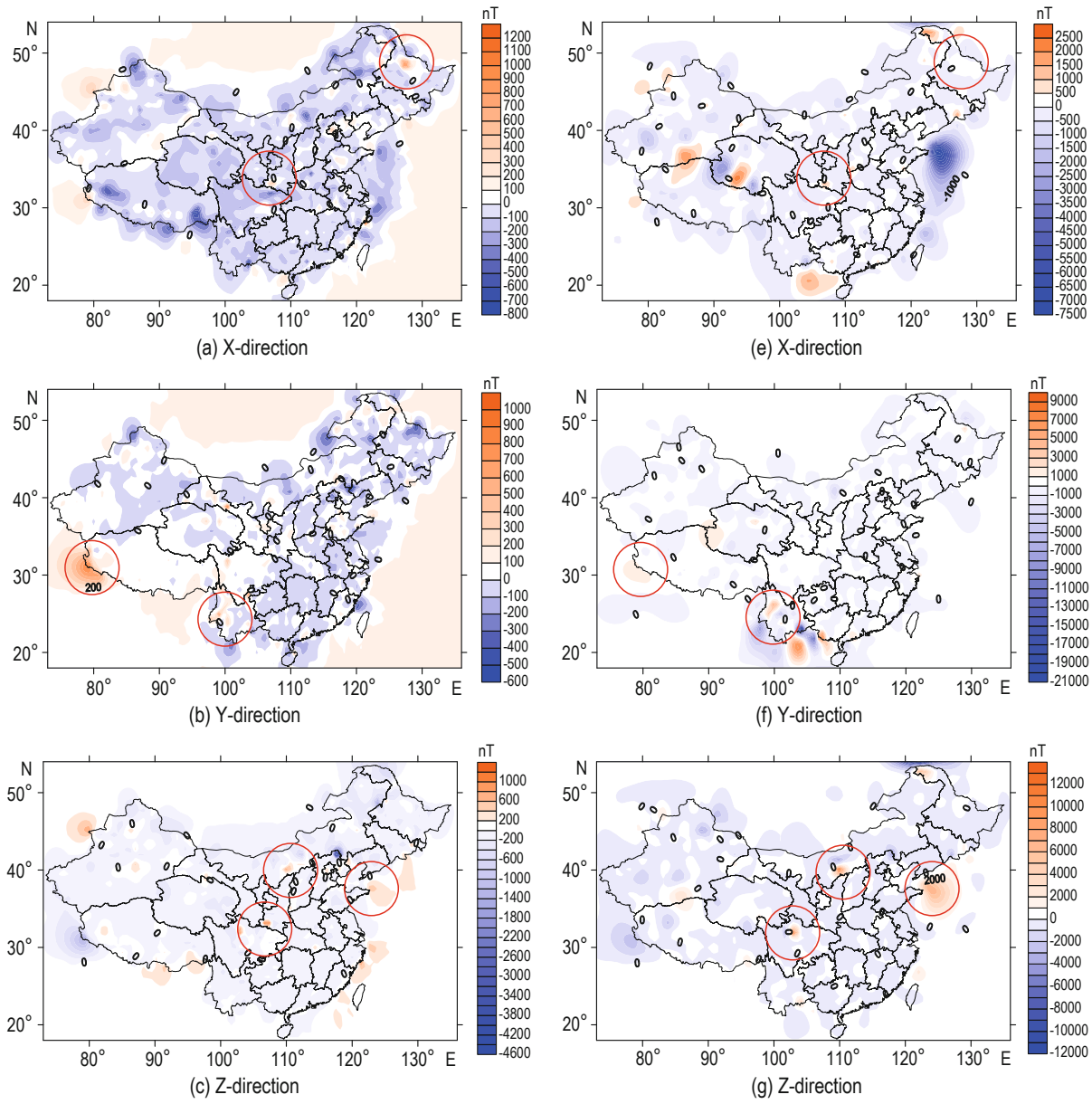

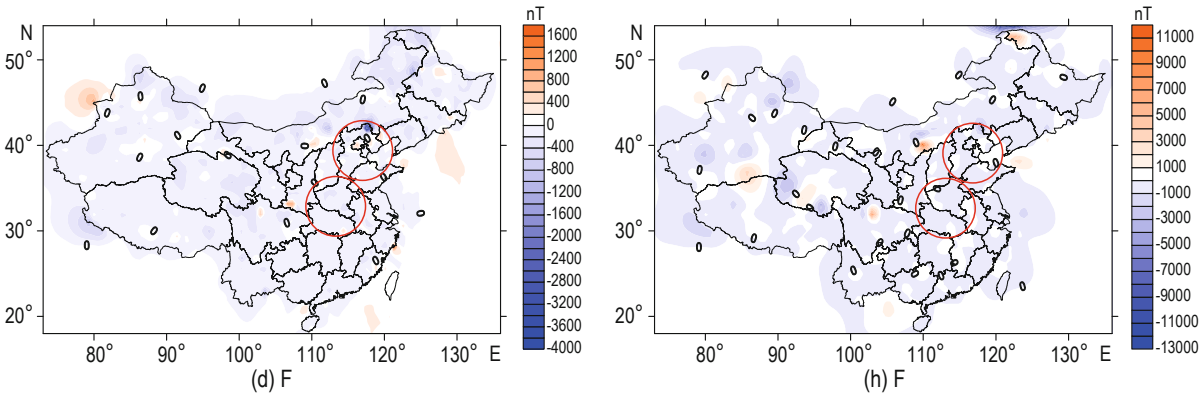

Fig.3 Anomaly distribution based on the measurement points (left) and SS (right). Magnetic intensity unit: nT

similar. This also means that the SS model can describe the actual distribution to some extent. However, there are several large anomalies in the figures of the SS model. Taking the X-direction, as an example, we see that there is a high negative anomaly at about −7500 nT in the eastern Shandong peninsula and, actually, there are seven points with amplitude slightly greater than 500 nT (subtract IGRF11 from the measurements). This is also seen in the Y-direction near the same location.

Owing to the large number of measurement points, the large difference between the number of domestic points (2730) and complementary points (150) outside the mainland, and the large intensity differences between several adjacent points, there are differences between the two methods.

Next, the 3DTP model is chosen to model the entire distribution of the anomalies. The truncation level of 3DTP is three and after comparing the root-mean-square error (RMSE) of each truncation level, we obtain 27 coefficients as in levels five and six of the typical TP model. Data other than latitude, longitude, and altitude, are also required as input. The altitude of all measurement points is assume to remain unchanged during 1960.0–2000.0, the gridded data with 1 arcmin resolution were from The Global Land One-kilometer Base Elevation project (http://www.ngdc.noaa.gov/mgg/topo/) and all corresponding altitude data were obtained by selecting the closest point (the nearest gridded points to measurement points), and the errors between the measurement points and modeling locations are less than 0.0083˚. We show the 3D distribution of the anomalies in the X-, Y-, and Z-direction, and F based on 3DTP in Figure 4.

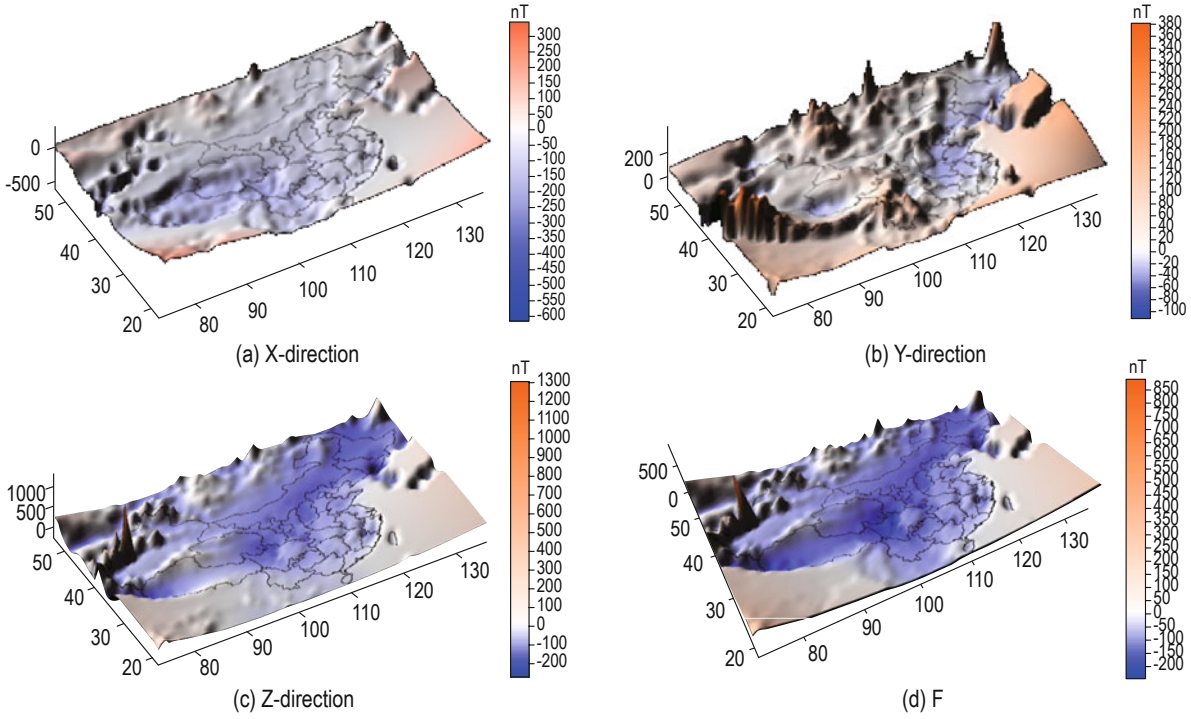

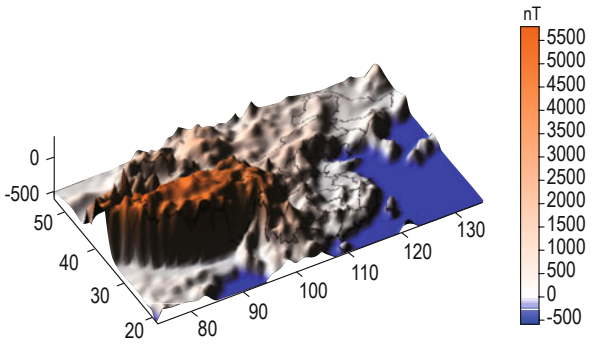

(e) Sea surface elevation field over the Chinese mainland

Fig.4 Anomaly distributions estimated by using the 3DTP model. Magnetic intensity unit: nT.

Comparing Figures 3 and 4, we see that the 3DTP model produces smoother and clearer distributions than the SS model, and is more consistent with KI, especially in the Y-direction. Moreover, the intensity of the anomalies is well controlled despite the obvious anomalies in western Tibet and southern Jilin. However, there positive anomalies in the X-direction in central Heilongjiang, and the negative anomalies in the Z-direction and F in northern Hebei are not distinguished. The intensity of the anomalies in the X-direction increases from about −100 nT to 0 nT with longitude, whereas in the Y-direction the intensity of the anomalies decreases from around 400 nT to 20 nT with longitude, and in the eastern mainland are almost negative. The intensities of the anomalies in the Z-direction and for F are highly similar and mostly about −50 nT, with the exception of western Tibet where the anomaly field is more negati

Conclusions

Based on measurements over the Chinese mainland in 1960.0, 1970.0, 1980.0, 1990.0, and 2000.0, we directly derived the anomalies based on KI and two regional models SS and 3DTP. The latter is a three-dimensional model and is used for the first time. The following conclusions were reached.

1. Anomalies of F based on SS and KI for different years are basically consistent in distribution and intensity, especially, for 1960.0, 1970.0, and 2000.0. The SS model produces more positive and negative anomalies.

2. We transfer all the measurements during 1960.0–1990.0 to 2000.0 and find that the anomalies are mainly negative (see also Feng, 2011). The intensity of the anomalies with the SS model is one order of magnitude higher than the intensity with KI. Nearly all extreme anomalous points are near or outside the boundaries, probably because of the large difference between the number of domestic and supplementary points and the lack of transition data

3. There are differences between the model distributions. The SS model reproduces the anomalies but creates extreme anomalies where the data are unevenly distributed. 3DTP produces smoother fitting and well suppresses the anomaly amplitudes but not all anomalies are suppressed.

Theoretically, the magnetic anomalies remain unchanged with time but spatiotemporal variations can take place over short periods. The different number of points and distribution of measurements in each year will produce differences in the simulated anomalies. Despite the differences between the three (KI, SS, 3DTP) model anomaly fields, their distributions are somewhat similar. The 3DTP model can estimate the regional magnetic field with improved precision relative to TP because of the added altitude term. Based on the SS model results, we observed extreme points with high intensities and whether these points are real or artificial requires in situ verification or higher precision models. Consequently, one can select a suitable model based on SS and 3DTP and the target. In the future, we plan to combine high-quality satellite data, such as SWARM constellations with marine and ground-based survey data, to derive high-quality anomaly models and extend their application.

Acknowledgements

We acknowledge the support of the staff of the Sate Key Laboratory of Space Weather, Chinese Academy of Sciences. We also wish to thank the reviewers for constructive comments.

References

An, Z. C., 1992a, Calculation and analysis of the gradient of the total geomagnetic intensity: Geophysical & Geochemical Exploration (in Chinese), **16**(5), 365−369.

An, Z. C., 1992b, Calculations and analyses of the horizontal gradient of the geomagnetic field: Advance in Earth Science (in Chinese), **7**(1), 39−43.

An, Z. C., 2000, Studies on geomagnetic field models of

Qinghai-Xizang plateau: Chinese Journal of Geophysics (in Chinese), **43**(3), 339−345.

An, Z. C., 2003, Spherical cap harmonic analysis of the geomagnetic residual field in China for 1950−1990: Chinese Journal of Geophysics (in Chinese), **46**(6), 767−771.

Feng, Y., 2011, Simulation of Lithospheric Magnetic Field over Chinese Mainland: Doctoral Dissertation. Nanjing Agricultural University, Nanjing.

Feng, Y., An, Z., Sun, H., and Mao, F., 2010a, Analysis of variation in geomagnetic field of Chinese mainland based on comprehensive model CM4: Acta Physica Sinsca (in Chinese), **59**(12), 8941−8953.

Feng, Y., An, Z., Sun, H., and Mao, F., 2010b, A study on model of geomagnetic normal field of China region: Advance in Earth Science (in Chinese), **25**(7), 723−729.

Gao, J., An, Z., Gu, Z., Han, W., Zhan, Z., and Yao, T., 2005, Selections of the geomagnetic normal field and calculations of the geomagnetic anomalous field: Chinese Journal of Geophysics (in Chinese), **48**(1), 56−62.

Gao, J., An, Z., Gu, Z., Han, W., Zhan, Z., and Yao, T., 2006, Distributions of the geomagnetic field and its secular variations expressed by the surface Spline method in China (a part) for 1900−1936. Chinese Journal of Geophysics (in Chinese), **49**(2), 398−407.

Gu, Z., An, Z., Gao, J., Zhan, Z., Yao, T., Han, W., and Chen, B., 2006a, Computation and analysis of the geomagnetic field model in China and its adjacent area for 2003: Acta Seismologica Sinica, **19**(2), 145−154.

Gu, Z., An, Z., Gao, J., Han, W., and Zhan, Z., 2004, Spherical cap harmonic analysis of the geomagnetic field in the Beijing-Tianjin-Hebei region: Chinese Journal of Geophysics (in Chinese), **47**(6), 1003−1008.

Gu, Z., Chen, B., Gao, J., Xin, C., Yuan, J., and Di, C., 2009, Research of geomagnetic spatial-temporal variation in China by NOC method: Chinese Journal of Geophysics (in Chinese), **52**(10), 2602−2612.

Gu, Z., Zhan, Z., Gao, J., Han, W., An, Z., Yao, T., and Chen, B., 2006b, Geomagnetic survey and geomagnetic model research in China: Earth Planets Space, **58**(6), 741−750.

Langel, R., Estes, R., and Mead G. D., 1982, Some new methods in geomagnetic field modeling a pplied to the 1960–1980 epoch: Journal of Geomagnetism and Geoelectricity, **34**(6), 327−349.

Langel, R. A., Sabaka, T. J., Baldwin, R. T., and Conrad, J. A., 1996, The near Earth magnetic field from magnetospheric and quiet-day ionospheric sources and how it is modeled: Physics of the Earth and Planetary Interiors, **98**(3−4) 235−267.

Liu, S. J., Zhou, X. G., Sun, H., and An, Z., 2011, The three dimension Taylor polynomial method for the calculation of regional geomagnetic: Process in Geophys. (in Chinese), **26**(4), 1165−1174.

Maus, S., 2010, An ellipsoidal harmonic representation of Earth's lithospheric magnetic field to degree and order 720, Geochemistry Geophysics Geosystems, **11**(6), Q06015.

Maus, S., Yin, F., Luhr, H., Manoj, C., Rother, M., Rauberg, J., Michaelis, I., Stolle, C., and Muller, R. D., 2008, Resolution of direction of oceanic magnetic lineations by the sixth-generation lithospheric magnetic field model from CHAMP satellite magnetic measurements: Geochemistry Geophysics Geosystems, **9**(7), 488−498.

Maus, S., Luhr, H., Rother, M., Hemant, K., Balasis, G., Ritter, P., and Stolle, C., 2007, Fifth-generation lithospheric magnetic field model from CHAMP satellite measurements: Geochemistry Geophysics Geosystems, **8**(5), 622−634.

Olsen, N., 1993, The solar cycle variability of lunar and solar daily geomagnetic variations: Ann. Geophys., **11**(4), 254−262.

Sabaka, T. J., Olsen, N., and Langel, R. A., 2002, A comprehensive model of the quiet-time, near-Earth magnetic field: phase 3: Geophys. J. Int., **151**(1), 32−68.

Sabaka, T. J., Olsen, N., and Purucker, M. E., 2004, Extending comprehensive models of the Earth's magnetic field with Ørsted and CHAMP data: Geophys. J. Int., **159**(2), 521−547.

Tschu, K., and Xu, W., 1985, A nested geomagnetic model of China and neighbouring region, Chinese Journal of Geophysics (in Chinese), **28**(2), 133−141.

Wang, Y., An, Z., Golovkov, V. P., Rotatnova, N. M., and Kharitonov, A. L., 1999, Theoretical analysis of geomagnetic field over east Asia and rectangular harmonic model: Chinese Journal of Geophysics (in Chinese), **42**(5), 640−647.

Xu, W., Xia, G., An, Z., Chen, G., Zhang, F., Wang, Y., Tian, Y., Wei, Z., Ma, S., and Chen, H., 2003, Magnetic survey and ChinaGRF 2000: Earth, Planets and Space, **55**(4), 215−217.

Feng Yan, Ph.D., is presently working at the College of Mathematics and Statistics, Nanjing University of Information Science & Technology. His research interests are modeling of regional and global geomagnetic fields, the secular variations and interrelations between geomagnetic fields and CMB, and the relation between geomagnetic field and space weather.